

Mechanistic insights and antifungal assessment of (3+2) cycloaddition products of 2-diazopropane and 5-hydroxy-3-methyl-1,5-dihydropyrrol-2-one derivatives

Abdeljabbar Jaddi^{a,b}, Amine Rafik^{a,c}, Saloua Sebbahi^a, Mohammed Salah^d and Khadija Marakchi^{a*}

^aLaboratory of Spectroscopy, Molecular Modelling, Materials, Nanomaterials, Water and Environment, LS3MN2E/CERNE2D, Faculty of Sciences, Mohammed V University in Rabat, Rabat, Morocco

^bInstituto de Física Fundamental, Consejo Superior de Investigaciones Científicas, Serrano 123, 28006 Madrid, Spain

^cDepartamento de Ciencias Integradas, Centro de Estudios Avanzados en Física, Matemática y Computación; Unidad Asociada GIFMAN, CSIC-UHU, Universidad de Huelva, Huelva, 21071, Spain

^dMolecular Modelling and Spectroscopy Research Team, Faculty of Science, Chouaib Doukkali University, P.O. Box 20, 24000, El Jadida, Morocco

CHRONICLE

Article history:

Received October 16, 2024

Received in revised form

November 2, 2024

Accepted March 19, 2025

Available online

March 19, 2025

Keywords:

(3+2) cycloaddition reaction

2-diazopropane

Pyrazoline

MEDT

Molecular docking

ABSTRACT

The (3+2) cycloaddition reactions of 2-diazopropane with derivatives of 5-hydroxy-3-methyl-1,5-dihydropyrrol-2-one were investigated using Molecular Electron Density Theory. Calculations were performed at the wB97XD/6-311++G(d,p) level of theory. Conceptual Density Functional Theory indices revealed a low polar character for these reactions, supported by a minimal global electron density transfer at the transition structures, which were classified as forward electron density flux processes. The Electron Localization Function analysis identified 2-diazopropane as a pseudo(mono)radical three-atom component. It further indicated that bond formation does not start at the transition structures. Mechanistically, these reactions proceed via an asynchronous one-step mechanism, ultimately leading to products that are kinetically favored. Furthermore, molecular docking studies were conducted to evaluate the antifungal potential of the reaction products against pathogenic fungal strains, *Candida albicans* and *Aspergillus fumigatus*. The docking analysis assessed binding affinities and characterized molecular interactions between the proposed compounds and critical fungal proteins, highlighting their potential as antifungal agents.

© 2025 by the authors; licensee Growing Science, Canada.

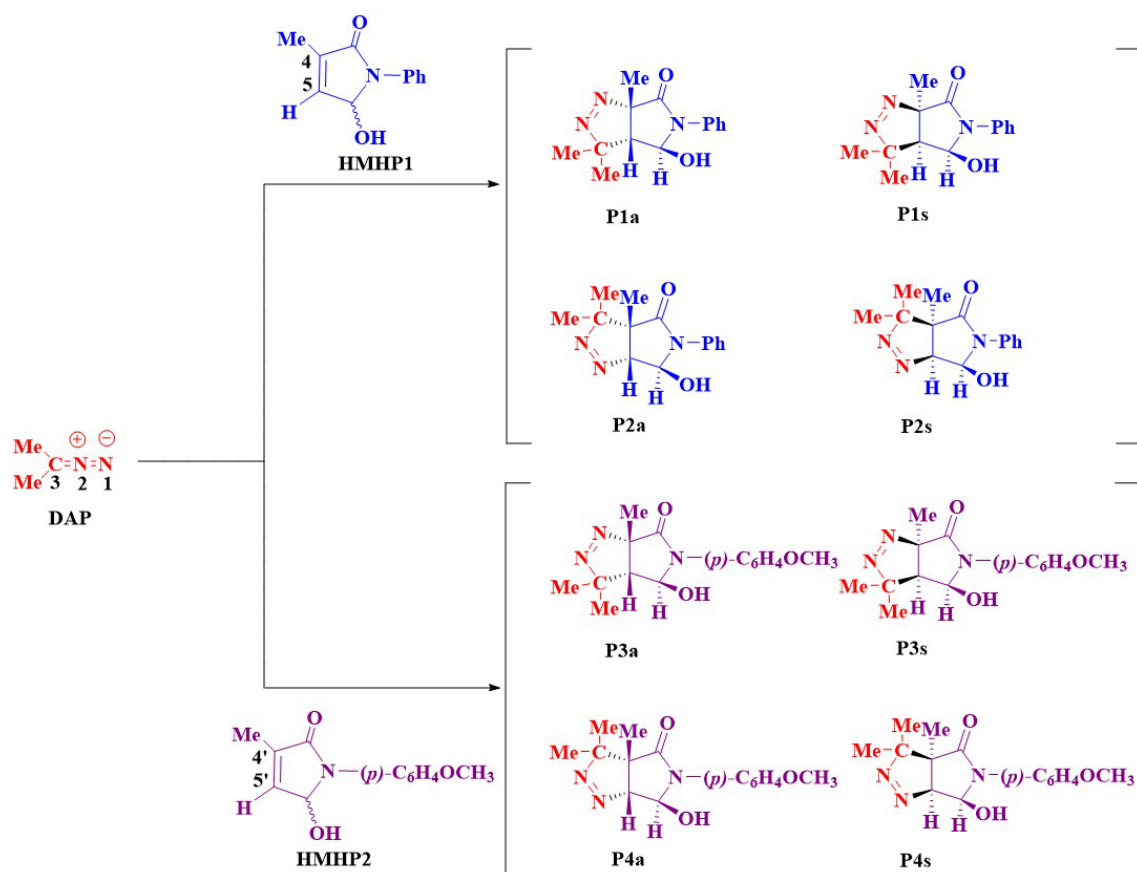
1. Introduction

The (3+2) cycloaddition (32CA) reactions are strong and flexible ways to control the regio- and stereoselective synthesis of chemical molecules with five atoms. With wide-ranging uses in pharmaceutical and medical chemistry as well as in materials science, these reactions have been rather helpful in the construction of sophisticated natural and synthetic scaffolds.¹ Three-atom components (TACs), which are made in situ as intermediates during 32CA reactions, have been studied in great detail by organic chemists. According to the new Molecular Electron Density Theory (MEDT),² TACs can be put into four groups: zwitterionic, carbenoid, pseudo(mono)radical, and pseudodiradical. These categories and their reactivity against ethylene³ have greatly progressed our knowledge of 32CA reactions. Due to their instability, the pseudo(mono)radical and pseudodiradical TACs exhibit particularly high responsiveness. Substitution plays a major role in altering the electronic structures and reactivity of TACs. Key TACs, like nitrilimines, are routinely used in 32CA reactions to make complex compounds, like pyrazoline derivatives, that have clear regio- and stereochemical properties.⁴⁻⁶ Many experimental and computational investigations have focused on the biologically active pyrazoline derivatives. These compounds, considered an important class in medicinal chemistry, have demonstrated biological effects such as antimicrobial,⁷ anti-inflammatory,⁸ antifungal,⁹ antimalarial,¹⁰ and anticancer agents.¹¹ MEDT is a new theory, that can be used to study how organic chemicals react with each other. MEDT states that changes in electron density, not molecular orbital interactions, define the core of chemical reactions. Since it was first conceived, MEDT has been used to explain

* Corresponding author

E-mail address k.marakchi@um5r.ac.ma (K. Marakchi)

chemical events like reactivity,^{3,12} selectivity,^{13,14} steric effects,¹⁵ and catalysis^{16,17} in a wide range of chemical systems and functional groups. This study looks at how the dipolar molecule 2-diazopropane (DAP) interacts with the dipolarophiles 5-hydroxy-3-methyl-1-phenyl-1,5-dihydro-2H-pyrrol-2-one (HMHP1) and 5-hydroxy-1-(4-methoxyphenyl)-3-methyl-1,5-dihydro-2H-pyrrol-2-one (HMHP2). Previous experimental results for these reactions give a basis for this study.¹⁸ We investigated four potential reaction paths using quantum-chemical methods to thoroughly study electron density variations in the MEDT framework (see **Scheme 1**). Topological studies using Electron Localization Function (ELF),^{19,20} Conceptual Density Functional Theory (CDFT),^{21,22} and Quantum Theory of Atoms in Molecules (QTAIM),²³ are some of the tools that are used. These methods help us to understand regioselectivity and stereoselectivity in organic reactions. This work explores the factors controlling the regio- and stereoselectivity of DAP reactions with HMHP1 and HMHP2, therefore clarifying the fundamental processes behind their selectivity. The goal is to develop selective synthetic methods for pyrazoline derivatives. Such derivatives have enormous medicinal potential, driven in part by the abuse and overuse of antibiotics in human health and agriculture, one urgent problem in therapeutic development is the rise of resistant bacteria. Among the fungal pathogens, *Aspergillus fumigatus* and *Candida albicans* are the most clinically important.²⁴ *Candida albicans* is a common commensal bacterium in the human microbiome. It can also be an opportunistic pathogen, which means it can cause both mild mucosal infections and severe life-threatening systemic candidacies.²⁵ On the other hand, *Aspergillus fumigatus* is mostly in charge of invasive aspergillosis, a severe infection mostly affecting immuno compromised people.²⁶ With only four main antifungal medication classes now accessible, advancements in antifungal therapies have been rare, despite the great demand over the past few decades. This inertia emphasizes the need for new therapeutic drugs to fight the increasing threat of resistant fungal pathogens.²⁷ This study looked at numerous designed compounds using in silico methods to find ones that might be able to kill *Candida albicans* and *Aspergillus fumigatus* fungi. Molecular docking simulations shed light on the binding affinities and interactions of these compounds with important fungal proteins, which promises leads for antifungal medication development.



Scheme 1. 32CA pathways of DAP with HMHP1 and HMHP2

2. Methods and Tools

2.1. Electronic structure calculations

Herein, we use the wB97XD DFT functional and the 6-311++G(d,p) basis set.^{28,29} We apply the Berny analytical gradient method³⁰ to determine the different stationary points along the reaction path. Vibrational frequency analysis proved the existence of transition structures (TSs) as stationary points by exposing a single imaginary frequency, which is a

distinguishing feature of TSs. The intrinsic reaction coordinate (IRC) calculations showed that the TSs were correctly linked to the reactant and product minima along the reaction path.³¹ Environmental effects were evaluated using gas phase calculations under the diethyl ether solvent (Et₂O). We investigated reactivity using conceptual density functional theory. The electronic chemical potential (μ) and chemical hardness (η) were calculated by using the frontier molecular orbital energies $\mu = (E_{\text{HOMO}} + E_{\text{LUMO}})/2$ and $\eta = E_{\text{LUMO}} - E_{\text{HOMO}}$.³² $\omega = \mu^2/2\eta$ represent the global electrophilicity index, which measures a molecule's ability to receive electrons. The global nucleophilicity index ($N = E_{\text{HOMO}}(\text{chemical compound}) - E_{\text{HOMO}}(\text{TCE})$)³³ was found using tetracyanoethylene (TCE) as reference, which gives a consistent scale for comparing nucleophilicities. A higher N value implies that the chemical has a stronger potential to donate electrons in nucleophilic interactions. Using Mulliken atomic spin densities,³⁴ Parr functions gave details about local reactions highlighting which parts of molecules are electrophilic and which parts are nucleophilic. $P_k^- = \rho_s^{\text{rc}}(k)$ and $P_k^+ = \rho_s^{\text{ra}}(k)$ represent Parr's indices. The Global Electron Density Transfer (GEDT)³⁵ is determined as follows: $\text{GEDT}(f) = \sum_{q \in f} q$. This value measures the

amount of electron density transfer between interacting molecule fragments at the TS, providing information about charge transport and polarization effects throughout the reaction. A greater GEDT value suggests considerable electron density transfer, which is commonly linked with polar transition structures. The molecular modeling was carried out using the GAUSSIAN 09 program.³⁶ The Multiwfn package³⁷ was used to find the parameters for QTAIM, Independent Gradient Model Hirshfeld (IGMH),³⁸ and Intrinsic Bond Strength Index for Weak Interactions (IBSIW).³⁹ The Topmod software⁴⁰ was used to do the ELF calculations. GaussView 6.0⁴¹ and the Visual Molecular Dynamics (VMD) package,⁴² have used for visualization throughout the work.

2.2. Molecular docking protocol

Molecular docking is a basic method to confirm and predict how a ligand will bind to its biological targets, especially when the affinity is high.⁴³ It gives information on the free energy binding properties and stability of the interactions. Early in the drug discovery phase, this procedure is absolutely essential for spotting intriguing candidates. AutoDock Vina,⁴⁴ was used to inspect how the 32CA reaction products interact with *Candida albicans* and *Aspergillus fumigatus*. The grid size for the receptor pockets is as follows: 1EAG ($x = 47.830, y = 18.841, z = 12.572$) and 3DJE ($x = 54.438, y = 0.326, z = 22.886$). We viewed and studied the docking data using the Molecular Operating Environment (MOE) program.⁴⁵ This gave a complete picture of the binding interactions and how they affected the antifungal activity.

3. Results and discussion

Herein, we start by analyzing the electronic characteristics of the reactants employing CDFT and ELF to elucidate the electronic properties of our reagents and the regioselectivity of our reactions. Then, we explore the energy profile of DAP with the two dipolarophiles HMHP1 and HMHP2. Following that, we calculate the charge transfer and electron density topologies at the TSs. Furthermore, we use the Bonding Evolution Theory (BET) method⁴⁶ in order to find the favored pathway of our reactions and reveal the bonds formation along them. Finally, we realize molecular docking studies for our 32CA products against *Candida albicans* and *Aspergillus fumigatus*.

3.1. Electronic properties of reagents

3.1.1. Global and local CDFT indices

Table 1 reports the four parameters (μ , η , ω , and N) for DAP, HMHP1, and HMHP2. The electronic chemical potential of DAP ($\mu = -3.28$ eV) is higher than that of HMHP1 ($\mu = -3.96$ eV) and HMHP2 ($\mu = -3.63$ eV), indicating a moderate electronic flux between the reactants. This result reflects the low polarity of these 32CA reactions. The electrophilicity index of DAP ($\omega = 0.64$ eV) categorizes it as a weak electrophile ($\omega < 0.80$ eV), whereas HMHP1 and HMHP2, with electrophilicity indices falling between (0.80 eV) and (1.16 eV), are classified as moderate electrophiles according to the standard electrophilicity scale.⁴⁷ In contrast, all three reactants exhibit nucleophilicity values exceeding 2.92 eV, which classifies them as strong nucleophiles.⁴⁷ Consequently, in these 32CA reactions, DAP acts predominantly as a nucleophile, while HMHP1 and HMHP2 function as electrophiles. These findings provide a detailed electronic perspective on the reactivity and interaction patterns of the reactants, paving the way for a deeper mechanistic understanding of the 32CA process.

Table 1. Global CDFT indices in eV of the DAP with HMHP1, and HMHP2 at the wb97XD/6-311++G(d,p).

	μ	η	ω	N
DAP	-3.28	8.36	0.64	4.02
HMHP1	-3.96	8.43	0.93	3.30
HMHP2	-3.63	7.95	0.83	3.87

The 32CA reaction will be between the electrophile's most electrophilic site and the nucleophile's most nucleophilic site. In order to find the nucleophilic and electrophilic sites (**Fig. 1**), we used the nucleophilic Parr functions from the DAP's

part, and electrophilic ones from the part of HMHP1 and HMHP2. The nucleophilic P_k^- functions show values of 0.60 and 0.51 on DAP's nitrogen atom N1 and carbon atom C3. On the other hand, with a value of 0.54, the carbon atom C5 is the most electrophilic site in HMHP1. Similarly, in HMHP2, the carbon atom C5' is valued at 0.58, making it more electrophilic than C4' (0.05). Thus, the favored interaction between the nitrogen N1 of DAP and the electrophile will take place between carbon C5 of HMHP1 and carbon C5' of HMHP2. These findings contradict the experiment.¹⁸ Thus, the approach of evaluating Parr functions at reagents doesn't work for this particular reaction, which can be explained by the relatively low polarity of the reaction.

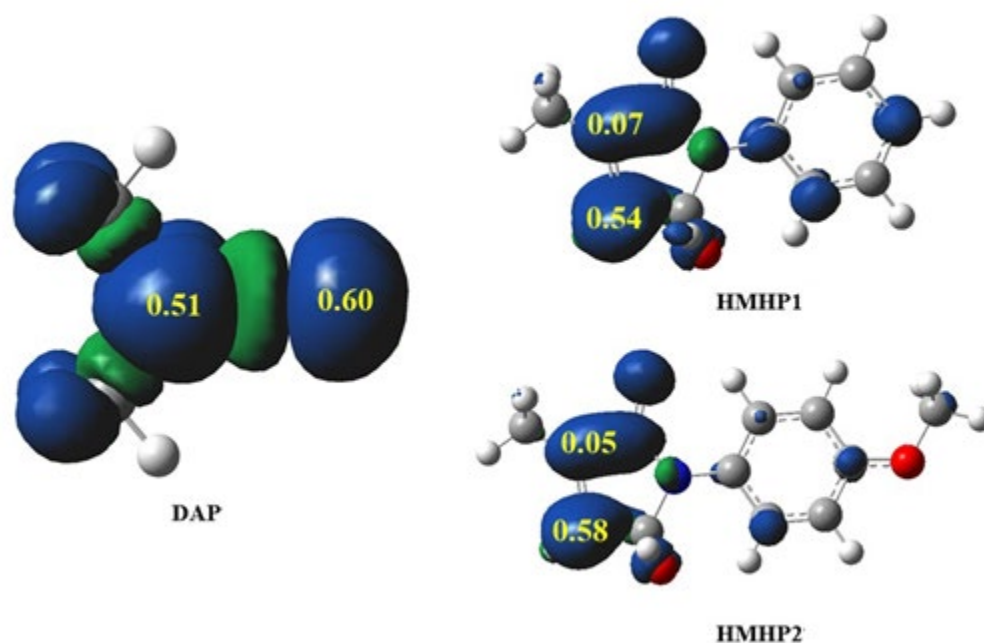


Fig. 1. P_k^- Parr functions of DAP and electrophilic P_k^+ Parr functions of HMHP1 and HMHP2

3.1.2. ELF topological analysis at the ground state of reactants

The results in the Supplementary Information (**Table 1S**) about the ELF valence basin populations is shown in terms of the average number of electrons, which makes it easy to see how many electrons are present. Adding a picture of the ELF localization areas, Lewis structures, and Natural Population Analysis (NPA) (**Fig. 1S**) helps to learn more about how the molecules of DAP, HMHP1, and HMHP2 react together. For DAP, we uncover two monosynaptic basins, $V(N1)$ and $V'(N1)$, holding 3.99 e, associated with the non-bonding electron density at N1 nitrogen that define the electronic structure at the N1-N2-C3 TAC framework. The disynaptic basins $V(N1, N2)$ and $V'(N1, N2)$ exhibit 3.50 e, which is associated with the N1-N2 double bond. Comparably, the $V(N2, C3)$ and $V'(N2, C3)$ basins include 3.30 e, linked to the N2-C3 double bond. With 0.94 e, two monosynaptic basins at C3, $V(C3)$ and $V'(C3)$ match the pseudoradical centering. Particularly, the two monosynaptic basins at C3 carbon integrate less than 1.0 e and are linked to a pseudoradical center C3,⁴⁸ which enables the pseudo(mono)radical TAC classification of DAP. In the ELF topological study of HMHP1, two disynaptic basins were found: $V(C4, C5)$ and $V'(C4, C5)$. These had a total electron population of 3.45 e indicating electron deficient C4-C5 double bonds. Two basins, $V(C4', C5')$ and $V'(C4', C5')$, with 3.45 e for HMHP2, match the underpopulated C4'-C5' double bond. These extensive ELF studies improve our knowledge of the electronic structure, bonding behavior, and molecular reactivity of DAP, HMHP1, and HMHP2 and will be employed as a reference subsequently in the analysis of the TSs. The charge distribution of the reactants is deduced from the NPA. The DAP's nitrogen N1 and carbon C3 atoms bear correspondingly negative charges of -0.12 e and -0.01 e, respectively. By contrast, nitrogen N2 has a positive charge of 0.04 e. The C5 carbon in HMHP1 shows a more marked negative charge of -0.18 e, whereas the C4 carbon has a charge of -0.06 e. Likewise, in HMHP2, C4' and C5' have charges of -0.07 e and -0.19 e, respectively.

3.2. Reaction energy profiles

3.2.1. Reaction of DAP with HMHP1

The 32CA reactions involving DAP and HMHP1 can occur through four pathways, resulting in two regioisomers, each available in both anti and syn stereoisomeric configurations. Analysis of the stationary points along the reaction coordinate

reveals that these 32CA reactions adhere to an asynchronous one-step mechanism. Four transition structures, TS1a, TS1s, TS2a, and TS2s, were identified along these pathways, leading to pyrazolines P1a, P1s, P2a, and P2s, as illustrated in **Scheme 1**. The relative enthalpies, entropies, and energies for the stationary points in the gas phase and Et₂O solvent at 273.15 K are given in the Supplementary Information (**Table 2S**). **Fig. 2** shows a plot of the relative energies. The negative reaction free energies for the 32CA reaction between DAP and HMHP1 range from -14.15 to -21.07 kcal.mol⁻¹ in the gas phase and from -13.29 to -21.51 kcal.mol⁻¹ in Et₂O solvent. This suggests that the reaction is exergonic. This means the reaction is thermodynamically favorable. The activation free energy of TS1a is more stable than that of TS2s, TS2s, and TS1s by 1.76, 3.20, and 3.93 kcal.mol⁻¹ in Et₂O solvent, respectively. This means that the most favorable path involves TS1a, which is exactly what the experiments showed.¹⁸ In the gas phase, the activation enthalpies connected to these 32CA reactions are 11.47 (TS1a), 14.80 (TS1s), 9.51 (TS2a), and 11.42 (TS2s) kcal.mol⁻¹; in Et₂O solvent, they are 10.72 (TS1a), 14.20 (TS1s), 11.67 (TS2a), and 13.12 (TS2s) kcal.mol⁻¹. The reaction enthalpies are exothermic between -30.42 and -36.40 kcal mol⁻¹ in the gas phase and between -30.19 and -37.08 kcal.mol⁻¹ in an Et₂O solvent. The reaction entropies are calculated between -55.71 and -60.81 cal.mol⁻¹.K⁻¹ in the gas phase and range from -57.02 to -61.97 cal.mol⁻¹.K⁻¹ in Et₂O solvent. The activation entropies range from -51.52 to -60.81 cal.mol⁻¹.K⁻¹ in the gas phase, while in Et₂O solvent they span -53.27 to -56.25 cal.mol⁻¹.K⁻¹. The fact that the solvent effect had to be taken into account in order to match the experiment shows how important the Et₂O solvent is to the stereoselectivity seen in these reactions.

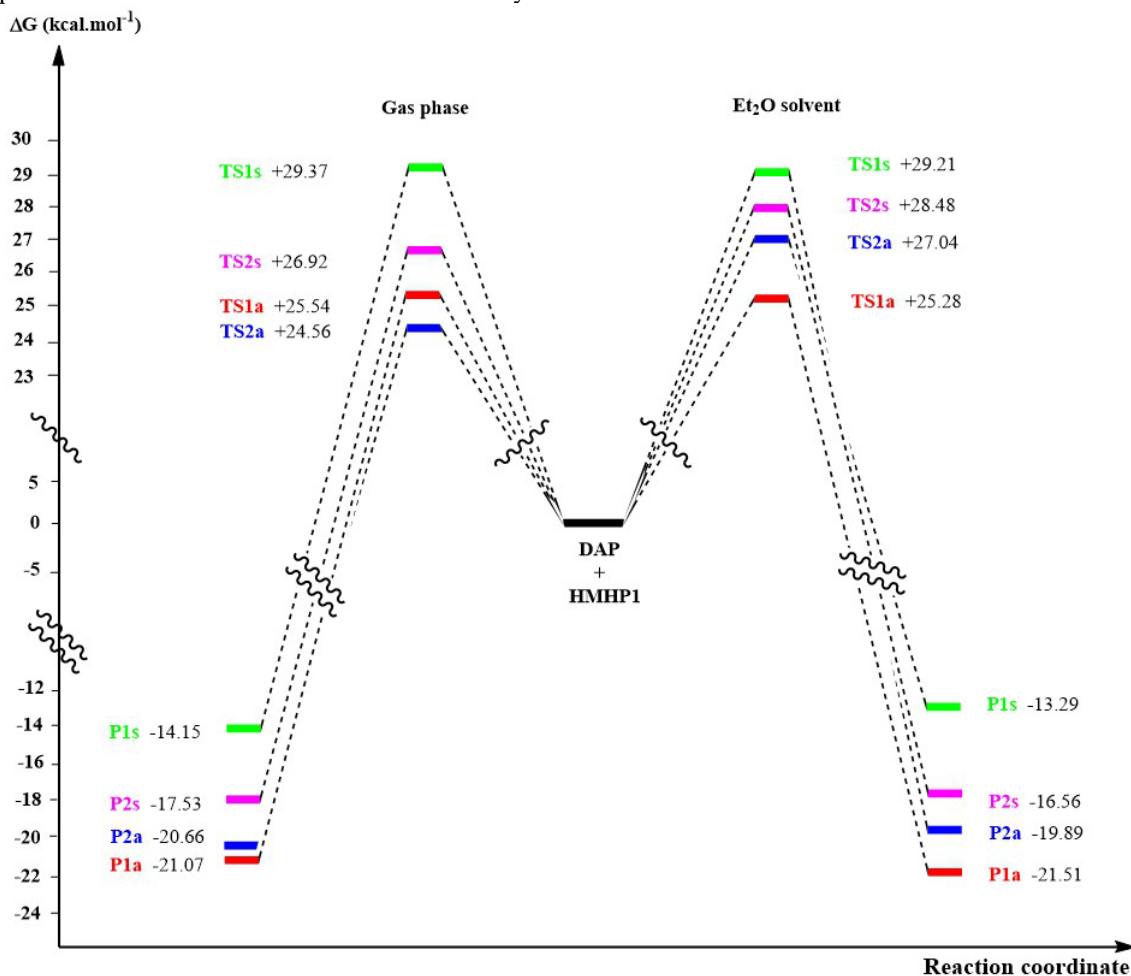


Fig. 2. Reaction energy paths for the 32CA reactions of DAP with HMHP1 in gas phase and in Et₂O solvent at 273.15 K

3.2.2. Reaction of DAP with HMHP2

The dipole's reaction with HMHP2 can also happen in four different pathways, as shown in **Scheme 1**. Each way involves two regioisomers and two stereoisomers. The Supplementary Information (**Table 3S**) provides the thermodynamic parameters of the stationary points in both the gas phase and Et₂O solvent at 273.15 K; a relative energy curve is shown in **Fig. 3**. The 32CA reaction between DAP and HMHP2 has a negative reaction free energy in both the gas phase and the Et₂O solvent. This means that the reaction is exergonic. It is clear that TS3a is the only one that works because its activation free energy is 2.54 kcal.mol⁻¹ lower than that of TS4a in the Et₂O solvent, which is exactly what the experiment showed.¹⁸ The activation enthalpies associated with these 32CA reactions have values between 10.19 and 14.34 kcal.mol⁻¹ in the gas phase while in Et₂O solvent they span from 10.42 to 14.25 kcal.mol⁻¹. In the gas phase, the reaction enthalpies are exothermic between -30.99 and -37.54 kcal.mol⁻¹; they fall in the range of -30.37 to -37.84 kcal.mol⁻¹ in Et₂O solvent. The solvent effect has to be taken into account in order to match the experimental results for how DAP interacts with HMHP1. Adding the

methoxy group to the para position of the phenyl group makes the HMHP2 derivative, but it doesn't change the selectivity seen at the level of the unsubstituted HMHP1 molecule.

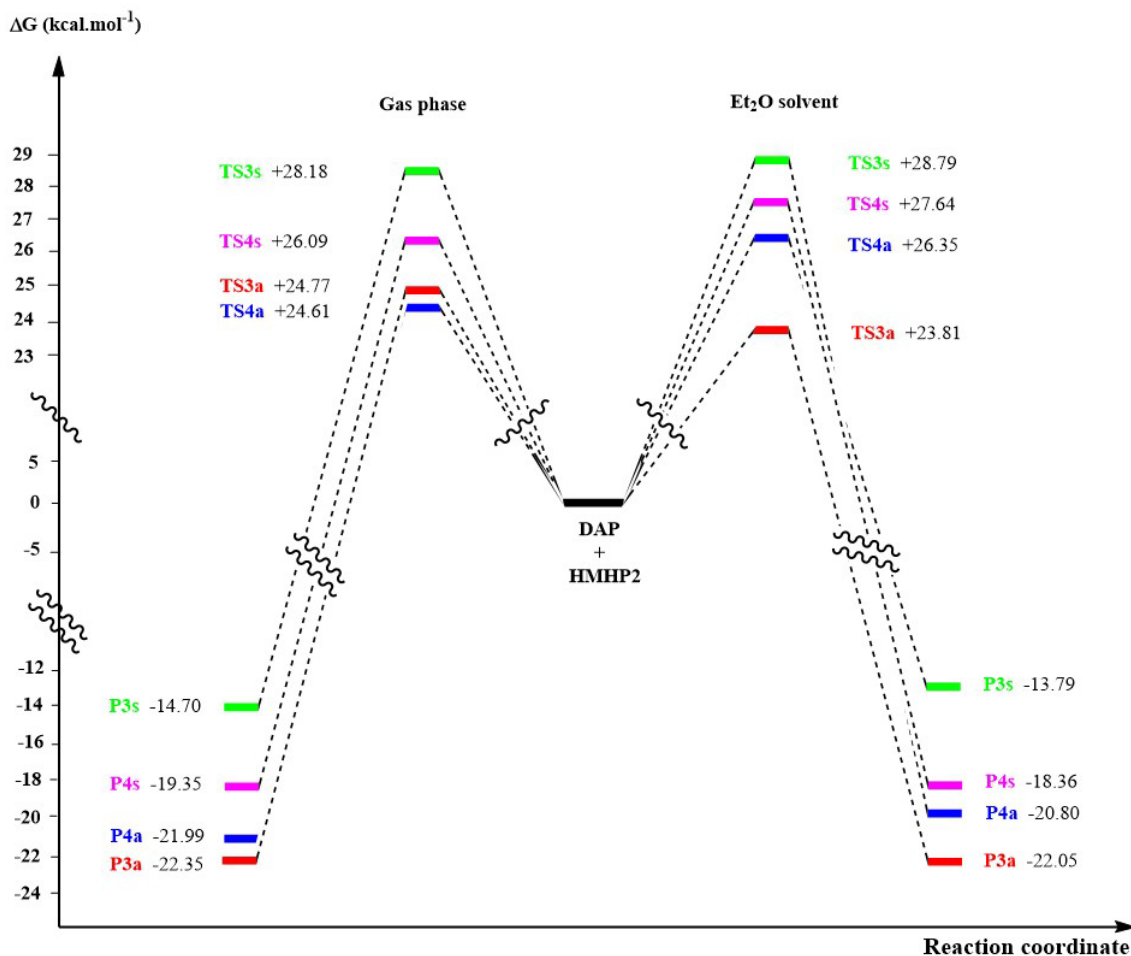


Fig. 3. Reaction energy paths for the 32CA reactions of DAP with HMHP2 in the gas phase and in Et₂O solvent at 273.15 K

3.2.3. Analysis of the bond distances at the TSs

By means of comparison between bond lengths in the TS and the resultant product, the index l gauges the asynchronicity of bond production in a chemical interaction. It is defined by the relation $l = 1 - \frac{r_{x-y}^{TS} - r_{x-y}^P}{r_{x-y}^P}$; r_{x-y}^{TS} and r_{x-y}^P are respectively the bond distances between atoms x and y in the TS and product respectively. The index l estimates the degree of advanced bond development at the TS. This index facilitates the knowledge of reaction processes and new sigma bond formation prediction. **Table 4S** shows the l indices for the reactions including DAP with HMHP1 and HMHP2 together with the bond distances in the TSs and products. At the level of the TS1a and TS1s, the C3-C5 sigma bond forms far more advanced during these 32CA reactions than the N1-C4 bond. The N1-C5 bond is therefore more advanced than the C3-C4 bond, implying a higher asynchronicity in bond formation for TS1a and TS2a than for TS1s and TS2s. This suggested a more asynchronous process in the anti approaches (TS1a and TS2a) than those connected with the syn approaches (TS1s and TS2s). This observation corresponds with the empirical rule seen in many Diels-Alder cycloadditions, whereby the TS with more asynchronicity shows a lower energy^{49,50} for dissymmetrically substituted dienophiles. All cases of DAP involving HMHP2 reactions show similar effects of asynchronous processes.

3.2.4. Analysis of global electron density transfer

We performed GEDT calculations at the TSs in order to investigate the polarity of 32CA reactions of the dipole DAP with dipolarophiles HMHP1 and HMHP2 (**Table 2**). Reactions with GEDT over 0.20 e are polar; those with GEDT below 0.05 e are non-polar. A modest polar reaction is suggested by the GEDT values of all the investigated TSs. These values lie between 0.16 e and 0.19 e in the gas phase and between 0.17 e and 0.20 e in the Et₂O solvent. Consistent with the electronic chemical potential values, the positive GEDT values show a forward electron density flux from the nucleophile DAP to the electrophiles HMHP1 and HMHP2 in coherence with the CDFT analysis.

Table 2. GEDT results in gas phase and in Et₂O solvent

		Gas phase	Et ₂ O
DAP + HMHP1	TS1a	0.18	0.20
	TS1s	0.17	0.19
	TS2a	0.19	0.19
	TS2s	0.16	0.17
DAP + HMHP2	TS3a	0.17	0.19
	TS3s	0.17	0.19
	TS4a	0.17	0.18
	TS4s	0.16	0.17

3.3. Topological analysis

3.3.1. ELF topological analysis at the ground state of TSs

ELF topology analysis enables one to evaluate electron density distribution at TSs and bond creation. While **Fig. 2S** shows the ELF localization domains matching TS1a, TS1s, TS2a, and TS2s, **Table 5S** includes the most important populations of valence basins at the TSs. The V(C3) monosynaptic basin with an integration of 0.84–0.95 e was found by the ELF analysis of the TSs, therefore revealing a pseudoradical center at C3. Furthermore, shown by the ELF study was a V(N2) monosynaptic basin connected to the non-bonding electron density at the nitrogen atom N2. Its overall population was 1.84–2.00 e. DAP did not show any indication of the non-bonding electron density at the N2 nitrogen. The two monosynaptic basins, V(N1) and V'(N1), which integrated 3.99 e at DAP, united into a single V(N1) monosynaptic basin at the TSs, integrating 3.67–3.76 e linked with the bonding region of N1. Likewise, the two disynaptic basins V(N2, C3) and V'(N2, C3), which integrated 3.30 e at DAP, merged into one V(N2, C3) disynaptic basin at the TSs, therefore integrating 1.92–1.98 e related to the N2–C3 bonding area. The two disynaptic basins V(C4, C5) and V'(C4, C5) united into a single V(C4, C5) disynaptic basin at the TSs after merging 3.45 e at HMHP1, merged into a single V(C4, C5) disynaptic basin at the TSs, integrating 3.04–3.35 e associated with the C4–C5 bonding region. Consequently, The TSs did not show V(N1, C4), V(N1, C5), V(C3, C4), or V(C3, C5) disynaptic basins, so indicating that the formation of new covalent bonds had not started at the TSs. The 32CA reaction between DAP and HMHP1 thus followed an asynchronous one-step mechanism.

Table 6S and **Fig. 3S** for all TSs in the reaction between DAP and HMHP2 show a similar trend whereby the presence of a V(C3) monosynaptic basin was observed integrating 0.84–0.96 e and showing the presence of a pseudoradical center at C3. Furthermore, the V(N2) monosynaptic basin found by the ELF study of the TSs integrated 1.84 to 2.01 e, matching the non-bonding electron density at the nitrogen atom N2. In particular, DAP lacked the non-bonding electron density at the N2 nitrogen. The V(N1) and V'(N1) basins with integrated 3.99 e in DAP combined into a single V(N1) monosynaptic basin at the TSs, with an integration of 3.68 to 3.75 e linked to the N1 bonding. The disynaptic basins V(N2, C3) and V'(N2, C3), initially integrating 3.30 e in DAP, merged into one V(N2, C3) disynaptic basin at the TSs, integrating 1.92 to 1.97 e, corresponding to the N2–C3 bond. The disynaptic basins V(C4', C5') and V'(C4', C5') at HMHP2, which had integrated 3.45 e, fused into a V(C4', C5') disynaptic basin at the TSs, integrating 3.04 to 3.36 e, linked with the C4–C5 bond. Thus, the lack of disynaptic basins V(N1, C4'), V(N1, C5'), V(C3, C4'), and V(C3, C5') suggested that the new covalent bonds had not developed at the TSs. As so, the reaction between DAP and HMHP2 followed an asynchronous one-step mechanism.

3.3.2. Bonding Evolution Theory study of the 32CA reaction between DAP with HMHP1 and QTAIM

By tracking the changes in electron density during the reaction pathway, the BET approach provides useful insights on chemical reactivity and lets one investigate bond evolution during the reaction mechanism. The mechanism was clarified by evaluating the ELF topology at several nuclear configurations along the most energy-efficient path for the 32CA reaction between DAP and HMHP1, hence guiding the pathway leading to the production of P1a. This pathway was split into five separate topological phases (I, II, III, IV, V, and VI) by means of crucial ELF catastrophes. While **Fig. 4S** depicts the relevant molecular structures and ELF attractor positions, **Table 7S** gives the ELF basin populations at several points along the IRC (P1–P7).

At P1, where d(N1–C4) is 3.07 Å and d(C3–C5) is 3.12 Å, the two fragments appear to be distinct reactants, as the basin values closely resemble those of the reactants after the transition structure; also noted at this time, the value of GEDT is 0.03 e. Two obvious variations are seen at P3, where d(N1–C4) is 2.36 Å and d(C3–C5) is 2.21 Å. On one hand, the formation of a monosynaptic basin V(N2) with an integrated population of 1.84 e and related to the non-bonding electron density at the nitrogen atom N2 marks this point. On the other hand, the two disynaptic basins V(C4,C5) and V'(C4,C5) combined to form a single V(C4,C5) disynaptic basin integrating 3.34 e. It is worth mentioning that TS1a is found in phase III. Furthermore, the lack of the disynaptic basins V(N1, C4) and V(C3, C5) at P3 and P4 indicates that, at these points, the production of new single bonds N1–C4 and C3–C5 has not begun yet. At the P5, the bond distances are d(N1–C4) = 2.03 Å and d(C3–C5) = 1.80 Å. Previously noted monosynaptic basins at C3 and C5 have vanished, and a new disynaptic basin V(C3,C5) has emerged with a total electron count of 1.73 e. This formation signifies the establishment of a C3–C5 single bond at 1.80 Å due to the coupling of the pseudoradical centres at C3 and C5. At P7, where d(N1–C4) is 1.49 Å and d(C3–

C5) is 1.54 Å, a noteworthy alteration results in the creation of the disynaptic basin $V(N1,C4)$, which integrates 1.80 e and is connected to the N1-C4 single bond. The absence of the monosynaptic basins at N1 and C4 suggests that the N1-C4 bond has been developed by means of interactions between the pseudoradical centers, now at a distance of 1.49 Å. This leads to a relaxation in molecular geometry and results in the formation of P1a.

The interatomic interactions at the TSs were projected using a topological study of the QTAIM. **Table 8S** evaluates the total electron density ρ and the Laplacian of electron density $\nabla^2\rho(r)$ in order to investigate the chemical processes at the crucial binding sites (BCPs), CP1 and CP2. At the level of the TSs in the 32CA reactions including DAP with HMHP1 and HMHP2, the production of new N-C bonds and C-C single bonds took a front stage. Values below 0.1 e found by the evaluation of electron density ρ at the crucial points CP1 and CP2 revealed non-covalent interactions. Moreover, the positive Laplacian electron density $\Delta^2\rho(r) > 0$ implied that covalent C-N and C-C single bonds had not yet started to develop in the TS. These results agree with the ELF analysis results.

3.3.3. IGMH analysis of the inter-fragment interactions

Fig. 4 and **Fig. 5** show the IGMH analysis results for DAP with HMHP1. Three distinct interaction types are highlighted by these results. The blue zone shows strong attractions; the green zone shows van der Waals (vdW) interactions; and the red zone shows significant repulsions. Covering the contact area between the fragments, a broad isosurface underlined non-covalent interactions at TS1a, TS1s, TS2a, and TS2s. The results show that the IGMH isosurface of TS1a was rather greater than those of TS1s, TS2a, and TS2s. The plot of TS1a shows a more significant blue and green zone, signifying strong vdW interactions and attractions, Furthermore, whilst the red zone was less strong, indicating less vdW repulsion forces in compared to the other TSs. This insight illustrates the reason the pathway connected by TS1a was more suitable. Thus, in line with experimental data, the cycloadduct P1a is the most favoured.

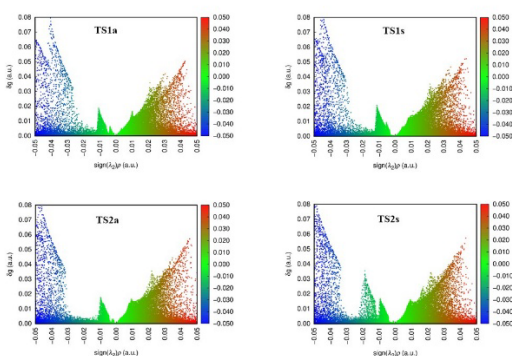


Fig. 4. Scatter plots of δg for the TSs associated with the 32CA reactions of DAP with HMHP1

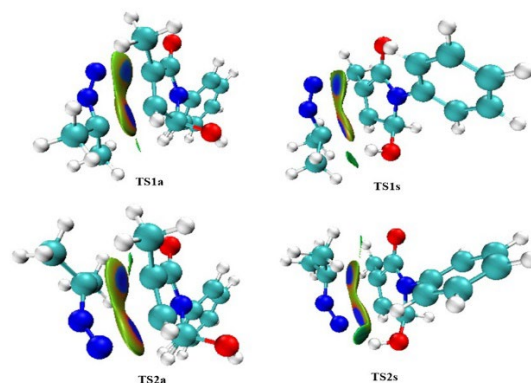


Fig. 5. $\text{Sign}(\lambda_2)\rho$ colored isosurfaces of $\delta g^{\text{inter}} = 0.015$ a.u. of TSs of the reaction of DAP with HMHP1. Blue is for attractive interactions, red is for repulsive interactions, and green is for Van der Waals forces

A comparable trend is observed in **Fig. 6** and **Fig. 7** regarding the reaction between DAP and HMHP2, where the results indicate that the IGMH isosurface of TS3a is marginally larger than those for TS3s, TS4a, and TS4s. This result indicates the favourability of the pathway connected through TS3a. The representation for TS3a features a more intense blue and green zone that highlights strong attraction and van der Waals (vdW) interactions, Whereas the rather less intense red zone shows relative repulsion forces relative to the other TSs. As so, P3a is preferred over P3s, P4a, and P4s products.

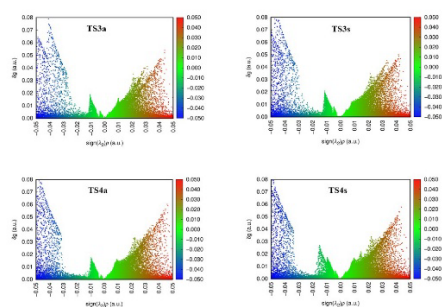


Fig. 6. Scatter plots of δg for the TSs associated with the 32CA reactions of DAP with HMHP2

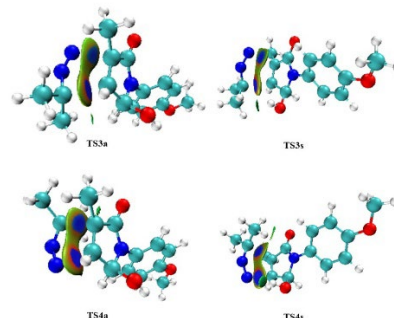


Fig. 7. $\text{Sign}(\lambda_2)\rho$ colored isosurfaces of $\delta g^{\text{inter}} = 0.015$ a.u. of TSs of the reaction of DAP with HMHP2. Blue is for attractive interactions, red is for repulsive interactions, and green is for Van der Waals forces

3.3.4. Intrinsic Bond Strength Index for Weak Interactions

Within chemical reactions, the IBSIW offers a quantitative assessment of the strength of weak interactions at TSs. Unlike strong covalent bonds, these weaker interactions often are more sensitive and vary greatly depending on the chemical environment. **Fig. 8** shows the IBSIW values for DAP with HMHP1 showing that the C3-C5 bond in TS1a and TS1s is more advanced than the N1-C4 bond, whereas in TS2a and TS2s, the N1-C5 bond is further along than the C3-C4 bond, pointing to an asynchronous bonding process. Likewise, the interaction of DAP with HMHP2, shown in **Fig. 9**, showed that in TS3a and TS3s the C3-C5' bond is more developed than the N1-C4' bond. Moreover, in TS4a and TS4s, the N1-C5' bond develops more than the C3-C4' bond. This aligns with the *l* index's aggregated past findings.

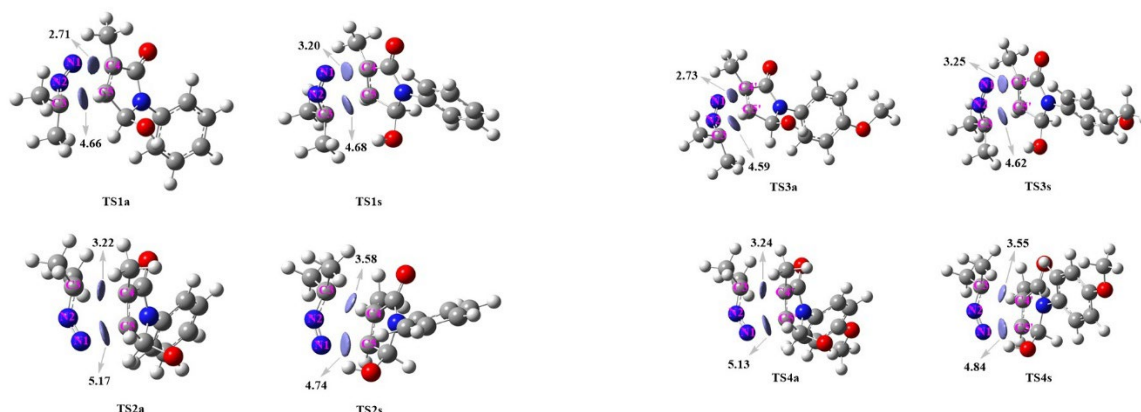


Fig. 8. IBSIW values for TSs of the reactions of DAP and HMHP1

Fig. 9. IBSIW values for TSs of the reactions of DAP and HMHP2

3.4. Molecular docking analysis

Binding processes between presumably bioactive molecules and target receptors are investigated via molecular docking. In this work we assess, against harmful fungus *Candida albicans* and *Aspergillus fumigatus*, the antifungal activity of the 32CA reaction products P1a, P1s, P2a, P2s, P3a, P3s, P4a, and P4s. The work assesses the binding affinities and investigates the molecular interactions these molecules create with pertinent fungus' proteins.

Table 3 shows the docking results of the 32CA reaction products against both fungal strains. They show that to some degree of all compounds interacting with the receptor proteins. Particularly, the product P4s has the highest expected binding energy to the receptor 3DJE, that is $-8.4 \text{ kcal}\cdot\text{mol}^{-1}$. Regarding the 1EAG receptor, at $-7.5 \text{ kcal}\cdot\text{mol}^{-1}$, the binding energy of the product P1s was the strongest. P4s is therefore identified as the product with most potential bioactivity against *Aspergillus fumigatus*, while P1s is reported as the product with most potential against *Candida albicans*.

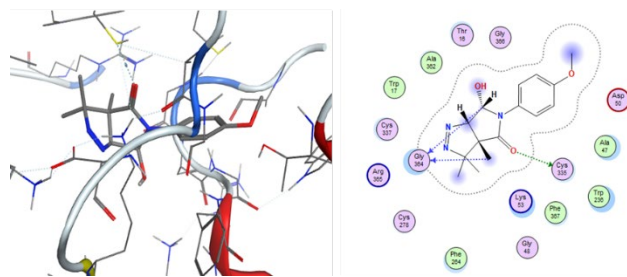
Table 3. The binding affinity of designed compounds ($\text{kcal}\cdot\text{mol}^{-1}$).

proteins	ligands							
	P1a	P1s	P2a	P2s	P3a	P3s	P4a	P4s
3DJE	-6.9	-7.9	-7.4	-8.1	-7.0	-7.2	-7.2	-8.4
1EAG	-7.3	-7.5	-6.7	-6.3	-6.6	-7.1	-7.2	-6.7

Table 4 gathers the features of the most important interactions between amino acids and ligands P4s and P1s. **Fig. 10** demonstrate the docking engagement of the ligand P4s with the 3DJE protein target in both two- and three-dimensional perspectives. For 3DJE, these interactions combine H-donor interactions with the active site amino acids GLY 364 (3.30 Å), CYS 335 (3.10 Å), and GLY 364 (3.16 Å). The P1s molecule is associating with the active site via an H-donor with amino acid GLY 220 (3.33 Å) and from an H-acceptor with THR 221 (2.87 Å) for 1EAG (**Fig. 11**).

Table 4. Interactions between ligands P4s and P1s with amino acids.

Proteins	Ligands	Amino acids	Interactions Types	Distances (Å)
3DJE	P4s	GLY 364	H-donor	3.16
		CYS 335	H-donor	3.10
		GLY 364	H-donor	3.30
1EAG	P1s	GLY 220	H-donor	3.33
		THR 221	H-acceptor	2.87



- Stereoselective Synthesis of Polycyclic Derivatives and Their Biological Testing. *Int J Mol Sci.*, 25, 11435. <https://doi.org/10.3390/ijms252111435>
6. Boukamcha N., Gharbi R., Martin M. -T., Chiaroni A., Mighri Z., and Khemiss A. (1999) Stereoselectivity and chemoselectivity in 1,3-dipolar cycloaddition reaction of 2-diazopropane with diarylidenacetones. *Tetrahedron*, 55, 449–460. [https://doi.org/10.1016/S0040-4020\(98\)01056-4](https://doi.org/10.1016/S0040-4020(98)01056-4)
 7. Almahdi M. M., Saeed A. E. M., and Metwally N. H. (2019) Synthesis and antimicrobial activity of some new pyrazoline derivatives bearing sulfanilamido moiety. *Eur J Chem.*, 10, 30–36. <https://doi.org/10.5155/eurjchem.10.1.30-36.1791>
 8. Andrew T. L., Cox J. R., and Swager T. M. (2010) Synthesis, Reactivity, and Electronic Properties of 6,6-Dicyanofulvenes. *Org Lett.*, 12, 5302–5305. <https://doi.org/10.1021/ol102384k>
 9. Hassan S. (2013) Synthesis, Antibacterial and Antifungal Activity of Some New Pyrazoline and Pyrazole Derivatives. *Molecules*, 18, 2683–2711. <https://doi.org/10.3390/molecules18032683>
 10. Ravindar L., Hasbullah S. A., Rakesh K. P., and Hassan N. I. (2023) Pyrazole and pyrazoline derivatives as antimalarial agents: A key review. *Eur J Pharm Sci.*, 183, 106365. <https://doi.org/10.1016/j.ejps.2022.106365>
 11. Haider K., Shafeeque M., Yahya S., and Yar M. S. (2022) A comprehensive review on pyrazoline based heterocyclic hybrids as potent anticancer agents. *Eur J Med Chem Rep.*, 5, 100042. <https://doi.org/10.1016/j.ejmcr.2022.100042>
 12. Domingo L. R., Ríos-Gutiérrez M., and Pérez P. (2018) A Molecular Electron Density Theory Study of the Reactivity and Selectivities in [3 + 2] Cycloaddition Reactions of C, N-Dialkyl Nitrones with Ethylene Derivatives. *J Org Chem.*, 83, 2182–2197. <https://doi.org/10.1021/acs.joc.7b03093>
 13. Acharjee N. (2020) Unravelling the regio- and stereoselective synthesis of bicyclic N,O-nucleoside analogues within the molecular electron density theory perspective. *Struct Chem.*, 31, 2147–2160. <https://doi.org/10.1007/s11224-020-01569-x>
 14. Domingo L. R., Ríos-Gutiérrez M., and Acharjee N. (2019) A Molecular Electron Density Theory Study of the Chemoselectivity, Regioselectivity, and Diastereofacial Selectivity in the Synthesis of an Anticancer Spiroisoxazoline derived from α -Santonin. *Molecules*, 24, 832. <https://doi.org/10.3390/molecules24050832>
 15. Domingo L., Acharjee N., and Mohammad-Salim H. (2020) Understanding the Reactivity of Trimethylsilyldiazoalkanes Participating in [3+2] Cycloaddition Reactions towards Diethylfumarate with a Molecular Electron Density Theory Perspective. *Organics*, 1, 3–18. <https://doi.org/10.3390/org1010002>
 16. Domingo L. R., and Acharjee N. (2018) [3+2] Cycloaddition Reaction of C-Phenyl- N-methyl Nitron to Acyclic-Olefin-Bearing Electron-Donating Substituent: A Molecular Electron Density Theory Study. *ChemistrySelect.*, 3, 8373–8380. <https://doi.org/10.1002/slct.201801528>
 17. Mondal A., Mohammad-Salim H. A., and Acharjee N. (2023) Unveiling substituent effects in [3+2] cycloaddition reactions of benzonitrile N-oxide and benzylideneanilines from the molecular electron density theory perspective. *Sci Radices*, 2, 75–92. <https://doi.org/10.58332/scirad2023v2i1a05>
 18. Ben Hamadi N., and Msaddek M. (2011) 1,3-dipolar cycloadditions of aryl nitrile oxides and 2-diazopropane with 5-hydroxy-3-methyl-1,5-dihydropyrrol-2-one derivatives. *Comptes Rendus Chim.*, 14, 891–895. <https://doi.org/10.1016/j.crci.2011.02.005>
 19. Becke A. D., and Edgecombe K. E. (1990) A simple measure of electron localization in atomic and molecular systems. *J Chem Phys.*, 92, 5397–5403. <https://doi.org/10.1063/1.458517>
 20. Silvi B., and Savin A. (1994) Classification of chemical bonds based on topological analysis of electron localization functions. *Nature*, 371, 683–686. <https://doi.org/10.1038/371683a0>
 21. Geerlings P., De Proft F., and Langenaeker W. (2003) Conceptual Density Functional Theory. *Chem Rev.*, 103, 1793–1874. <https://doi.org/10.1021/cr990029p>
 22. Domingo L., Ríos-Gutiérrez M., and Pérez P. (2016) Applications of the Conceptual Density Functional Theory Indices to Organic Chemistry Reactivity. *Molecules*, 21, 748. <https://doi.org/10.3390/molecules21060748>
 23. Bader R. F. W., and Essén H. (1984) The characterization of atomic interactions. *J Chem Phys.*, 80, 1943–1960. <https://doi.org/10.1063/1.446956>
 24. Fisher M. C., Alastruey-Izquierdo A., Berman J., Bicanic T., Bignell E. M., Bowyer P., Bromley M., Brüggemann R., Garber G., Cornely O. A., Gurr S. J., Harrison T. S., Kuijper E., Rhodes J., Sheppard D. C., Warris A., White P. L., Xu J., Zwaan B., and Verweij P. E. (2022) Tackling the emerging threat of antifungal resistance to human health. *Nat Rev Microbiol.*, 20, 557–571. <https://doi.org/10.1038/s41579-022-00720-1>
 25. Lopes J. P., and Lionakis M. S. (2022) Pathogenesis and virulence of *Candida albicans*. *Virulence*, 13, 89–121. <https://doi.org/10.1080/21505594.2021.2019950>
 26. Shinu P., Gupta G. L., Sharma M., Khan S., Goyal M., Nair A. B., Kumar M., Soliman W.E., Rahman A., Attimarad M., Venugopala K. N., and Altaweel A. A. A. (2023) Pharmacological Features of 18 β -Glycyrrhetic Acid: A Pentacyclic Triterpenoid of Therapeutic Potential. *Plants*, 12, 1086. <https://doi.org/10.3390/plants12051086>
 27. Arastehfar A., Carvalho A., Houbraken J., Lombardi L., Garcia-Rubio R., Jenks J. D., Rivero-Menendez O., Aljohani R., Jacobsen I. D., Berman J., Osheroov N., Hedayati M. T., Ilkit M., Armstrong-James D., Gabaldón T., Meletiadis J., Kostrzewa M., Pan W., Lass-Flörl C., Perlin D. S., and Hoenigl M. (2021) *Aspergillus fumigatus* and aspergillosis: From basics to clinics. *Stud Mycol.*, 100, 100115–100115. <https://doi.org/10.1016/j.simyco.2021.100115>
 28. Calais J. (1993) Density-functional theory of atoms and molecules. R.G. Parr and W. Yang, Oxford University Press, New York, Oxford, 1989. IX + 333 pp. Price £45.00. *Int J Quantum Chem.*, 47, 101–101. <https://doi.org/10.1002/qua.560470107>

29. Chai J.-D., and Head-Gordon M. (2008) Long-range corrected hybrid density functionals with damped atom–atom dispersion corrections. *Phys Chem Chem Phys.*, 10, 6615. <https://doi.org/10.1039/b810189b>
30. Schlegel H. B. (1982) Optimization of equilibrium geometries and transition structures. *J Comput Chem.*, 3, 214–218. <https://doi.org/10.1002/jcc.540030212>
31. Gonzalez C., and Schlegel H. B. (1989) An improved algorithm for reaction path following. *J Chem Phys.*, 90, 2154–2161. <https://doi.org/10.1063/1.456010>
32. Pearson R. G. (1992) The electronic chemical potential and chemical hardness. *J Mol Struct THEOCHEM*, 255, 261–270. [https://doi.org/10.1016/0166-1280\(92\)85014-C](https://doi.org/10.1016/0166-1280(92)85014-C)
33. Domingo L. R., and Pérez P. (2011) The nucleophilicity N index in organic chemistry. *Org Biomol Chem.*, 9, 7168. <https://doi.org/10.1039/c1ob05856h>
34. Domingo L. R., Pérez P., and Sáez J. A. (2013) Understanding the local reactivity in polar organic reactions through electrophilic and nucleophilic Parr functions. *RSC Adv.*, 3, 1486–1494. <https://doi.org/10.1039/C2RA22886F>
35. Domingo L. R. (2014) A new C–C bond formation model based on the quantum chemical topology of electron density. *RSC Adv.*, 4, 32415–32428. <https://doi.org/10.1039/C4RA04280H>
36. Frisch M. J., Trucks G. W., Schlegel H. B., Scuseria G. E., Robb M. A., Cheeseman J. R., Scalmani G., Barone V., Mennucci B., Petersson G. A., Nakatsuji H., Caricato M., Li X., Hratchian H. P., Izmaylov A. F., Bloino J., Zheng G., Sonnenberg J. L., Hada M., Ehara M., Toyota K., Fukuda R., Hasegawa J., Ishida M., Nakajima T., Honda Y., Kitao O., Nakai H., Vreven T., Montgomery J. A. Jr., Peralta J. E., Ogliaro F., Bearpark M., Heyd J. J., Brothers E., Kudin K. N., Staroverov V. N., Kobayashi R., Normand J., Raghavachari K., Rendell A., Burant J. C., Iyengar S. S., Tomasi J., Cossi M., Rega N., Millam J. M., Klene M., Knox J. E., Cross J. B., Bakken V., Adamo C., Jaramillo J., Gomperts R., Stratmann R. E., Yazyev O., Austin A. J., Cammi R., Pomelli C., Ochterski J. W., Martin R. L., Morokuma K., Zakrzewski V. G., Voth G. A., Salvador P., Dannenberg J. J., Dapprich S., Daniels A. D., Farkas O., Foresman J. B., Ortiz J. V., Cioslowski J., and Fox D. J. (2009) Gaussian 09, Revision A.02, Gaussian, Inc., Wallingford CT.
37. Lu T., and Chen F. (2012) Multiwfn: A multifunctional wavefunction analyzer. *J Comput Chem.*, 33, 580–592. <https://doi.org/10.1002/jcc.22885>
38. Lu T., and Chen Q. (2022) Independent gradient model based on Hirshfeld partition: A new method for visual study of interactions in chemical systems. *J Comput Chem.*, 43, 539–555. <https://doi.org/10.1002/jcc.26812>
39. Rafik A., Jaddi A., Salah M., Komiha N., Carvajal M., and Marakchi K. (2024) Insights into the mechanism, selectivity, and substituent effects in the Diels-Alder reaction of azatrienes with electron-rich dienophiles: An MEDT study. *J Mol Graph Model.*, 132, 108819. <https://doi.org/10.1016/j.jmgm.2024.108819>
40. Noury S., Krokidis X., Fuster F., and Silvi B. (1999) Computational tools for the electron localization function topological analysis. *Comput Chem.*, 23, 597–604. [https://doi.org/10.1016/S0097-8485\(99\)00039-X](https://doi.org/10.1016/S0097-8485(99)00039-X)
41. Dennington R., Keith T. A., and Millam J. M. (2016) GaussView, Version 6.1. Semichem Inc., Shawnee Mission, KS.
42. Humphrey W., Dalke A., and Schulten K. (1996) VMD: Visual molecular dynamics. *J Mol Graph.*, 14, 33–38. [https://doi.org/10.1016/0263-7855\(96\)00018-5](https://doi.org/10.1016/0263-7855(96)00018-5)
43. Agu P. C., Afiukwa C. A., Orji O. U., Ezech E. M., Ofoke I. H., Ogbu C. O., Ugwuja E. I., and Aja P. M. (2023) Molecular docking as a tool for the discovery of molecular targets of nutraceuticals in diseases management. *Sci Rep.*, 13, 13398. <https://doi.org/10.1038/s41598-023-40160-2>
44. Trott O., and Olson A. J. (2010) AutoDock Vina: Improving the speed and accuracy of docking with a new scoring function, efficient optimization, and multithreading. *J Comput Chem.*, 31, 455–461. <https://doi.org/10.1002/jcc.21334>
45. Vilar S., Cozza G., and Moro S. (2008) Medicinal Chemistry and the Molecular Operating Environment (MOE): Application of QSAR and Molecular Docking to Drug Discovery. *Curr Top Med Chem.*, 8, 1555–1572. <https://doi.org/10.2174/156802608786786624>
46. Krokidis X., Noury S., and Silvi B. (1997) Characterization of Elementary Chemical Processes by Catastrophe Theory. *J Phys Chem A.*, 101, 7277–7282. <https://doi.org/10.1021/jp9711508>
47. Ríos-Gutiérrez M., Saz Sousa A., and Domingo L. R. (2023) Electrophilicity and nucleophilicity scales at different DFT computational levels. *J Phys Org Chem.*, 36, e4503. <https://doi.org/10.1002/poc.4503>
48. Domingo L. R., and Sáez J. A. (2011) Understanding the Electronic Reorganization along the Nonpolar [3 + 2] Cycloaddition Reactions of Carbonyl Ylides. *J Org Chem.*, 76, 373–379. <https://doi.org/10.1021/jo101367v>
49. Domingo L. R. (1999) Theoretical Study of the 1,3-Dipolar Cycloaddition Reactions of Azomethine Ylides. A DFT Study of Reaction between Trifluoromethyl Thiomethyl Azomethine Ylide and Acronitrile. *J Org Chem.*, 64, 3922–3929. <https://doi.org/10.1021/jo9822683>
50. Marakchi K., Ghailane R., Kabbaj O. K., and Komiha N. (2014) DFT study of the mechanism and stereoselectivity of the 1,3-dipolar cycloaddition between pyrroline-1-oxide and methyl crotonate. *J Chem Sci.*, 126, 283–292. <https://doi.org/10.1007/s12039-013-0563-y>

